Chapter 5. Earthquake Hazard Assessment

5-1 Scenario Earthquakes

5-1-1 Active Faults and Seismotectonic Modeling

The following faults have been identified and considered in terms of their seismotectonic impact within present-day patterns of deformation in the study area (Figure 5-1). The length, width and slip rate were modeled.

(1) Sahel Fault

The Sahel fault forms the boundary between the Mitidja basin to the south and the Sahel of Algiers to the north. Nevertheless, as the deep geometry of the fault is not known, we consider a rupture along the entire fault length, i.e. approx. 75 km (with all segments merging at depth and rupturing together). We also assume that the Sahel fault extends downward to a depth of 15 km. According to topographic response to displacement along the Sahel fault, it is estimated that slip rate should be in the order of a few tenths of a mm per year. For this Study, a slip rate of 0.5 ± 0.2 mm/yr will be assumed along the Sahel fault.

(2) Chenoua Fault

The Chenoua fault bounds the Chenoua massif to the south and extends offshore in a northeast direction. According to bathymetric data from the MARADJA cruise and instrumental seismicity, it is considered that the Chenoua fault has an approximate length of 50 km and a northwest dip of 45°. For this Study, a slip rate of 0.5 ± 0.2 mm/yr will be assumed along the Chenoua fault.

(3) Blida Fault

The Blida (south Mitidja) Fault marks the boundary between the Mitidja basin to the north and the Blidean Atlas to the south. As segmentation at depth is not known, we will assume that the Blida fault segments identified in the topography merge at depth and form a single segment with an approximate length of 90 km. It is also assumed that the Blida fault extends to a depth of 20 km. For this Study, a slip rate of 2.5 ± 1.0 mm/yr is assumed along the Blida fault.

(4) Offshore Active Faulting along the Algerian Margin

Recent offshore bathymetric and seismic reflection data from the MARADJA cruise (Deverchères et al., 2005) imaged the trace of this offshore fault along the base of the continental slope north of Zemmouri. Bathymetric data from the MARADJA cruise show a westward extension of this Zemmouri offshore fault not farther than the approximate longitude of Cape Matifou. However, additional data from the MARADJA cruise west of Algiers Bay (Domzig et al., submitted) show a similar major south dipping offshore fault following the base of the continental slope north of the Khair al Din bank. Bathymetric data show an eastward extension of this fault to the approximate longitude of Ain Benian. Even though there is no bathymetric evidence to show eastward extension of the fault trace to the Algiers Bay, we consider that this Khair al Din offshore fault should extend at depth beneath at least part of the Study Area. Segmentation for both offshore faults is unknown, but a

possible rupture along the entire length of each of these structures, i.e. approximately 100 km for the Zemmouri offshore fault and approximately 100 km for the Khair al Din offshore fault, is assumed. It is assumed that these two major structures extend to a depth of 20 km. As for the Blida fault, the Khair al Din offshore fault could accommodate, at the most, about half the total Africa-Eurasia convergence, i.e. a slip rate of 2.5 ± 1.0 mm/yr along the Khair al Din offshore fault. The Zemmouri offshore fault could potentially accommodate the largest part of the total Africa-Eurasia convergence, i.e. a slip rate of 4.0 ± 1.0 mm/yr along the Zemmouri offshore fault.

(5) Thenia Fault

The Thenia fault runs in a WNW-ESE direction near Boumerdes City. It extends from Algiers Bay to the Oued Isser over a total length of approximately 35 km. For this Study, a slip rate of 0.75 ± 0.25 mm/yr along the Thenia fault is assumed.

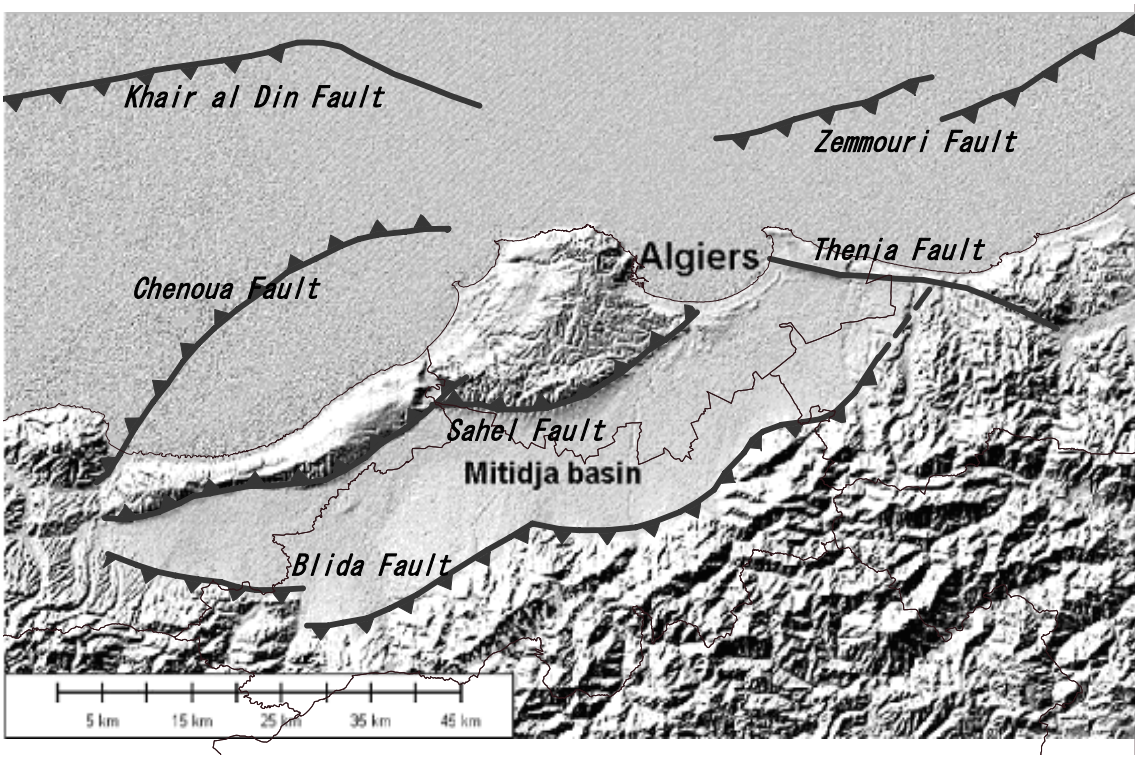

Figure 5-1 Location and Inferred Surface Traces of Faults
(Background Image: SRTM DEM)

5-1-2 Magnitude Modeling

(1) Maximum Magnitude

The magnitude of MCE (Maximum Credible Earthquake) on each identified active fault was derived using relationships between moment magnitude and area of rupture from Wells & Coppersmith (1994). These values are summarized in Table 5-1.

(2) Magnitude versus Return Period

A probabilistic approach does not seem pertinent to the Algiers area since earthquake sampling is very poor in terms of density, time frame and magnitude. Such an approach would result in a dilution of the hazard over large source areas.

A purely historical (deterministic) approach, implying the need to locate the Maximum Historical Earthquake at a more critical location along the fault, also does not seem pertinent because it would result in a very conservative hazard independent of any return periods.

We propose to mix probabilistic and deterministic approaches focusing on hazard controlled by identified active faults through models developed by Youngs and Coppersmith (1985). The magnitudes for a given return period appropriate for urban planning are determined.

The magnitude (m^o) for mean return period (T_m) along each identified active fault was estimated by following formula.

$$m^0 = m^u - \frac{1}{b \cdot \ln 10} \ln\left[1 + \frac{N(m^0) b Mo^u}{(1.5 - b)\mu A_f S}\right]$$

where m^u is the maximum magnitude, b is the b-value of the G-R relation, $N(m^o) = 1/T_m$, Mo^u is the seismic moment corresponding to the magnitude m^o, μ is the rigidity, A_f is the total fault plane area and S is the average slip rate along the fault.

Table 5-1 below summarizes the magnitudes associated with a 475 year return period for each critical seismogenic source and the parameters, deduced from the seismogenic context, that were used to estimate these magnitudes.

Table 5-1 Magnitudes Associated with a 475 Year Return Period for Critical Seismogenic Sources in the Algiers Area

Seismic Source	Upper Bound Magnitude (Mw)	Rupture Area (km^2)	Slip Rate (mm/yr)	Mw for 475 yr return period
Sahel Fault	7.2 ± 0.3	1590 ± 210	0.5 ± 0.2	5.9 ± 0.3
Chenoua Fault	7.0 ± 0.3	1060 ± 210	0.5 ± 0.2	5.8 ± 0.3
Blida Fault	7.4 ± 0.3	2545 ± 280	2.5 ± 1.0	6.8 ± 0.2
Khair al Din Fault	7.4 ± 0.3	2830 ± 565	2.5 ± 1.0	6.8 ± 0.2
Zemmouri Fault	7.4 ± 0.3	2830 ± 565	4.0 ± 1.0	7.0 ± 0.1
Thenia Fault	6.8 ± 0.3	600 ± 150	0.75 ± 0.25	5.9 ± 0.2

[References]

Deverchère J., Yelles K., Domzig A., Mercier de Lepinay B., Bouillin J.P., Gaullier V., Bracène R., Calais E., Savoye B., Kherroubi A., Le Roy P., Pauc H., and Dan G., 2005. Active thrust faulting offshore Boumerdes, Algeria, and its relation to the 2003 Mw 6.9 earthquake. Geophysical Research Letters, v. 32, L04311

Domzig A., Le Roy C., Yelles K., Deverchère J., Bouillin J-P., Bracene R., Mercier de Lèpinay B., Le Roy P., Calais E., Kherroubi A., Gaullier V., Savoye B., and Pauc H, submitted. Africa-Eurasia Miocene

collision and neotectonics offshore Algeria: Preliminary results from the MARADJA cruise. Under review for publication in C.R. Géosciences (July 2005).

Wells D.L., & Coppersmith K.J., 1994, New empirical relationships among Magnitude, Rupture Length, Rupture Width, Rupture Area and Surface Displacement. Bulletin of the Seismological Society of America, 84, pp. 974-1002.

Youngs R. R. and Coppersmith K. J., 1985, Implications of fault slip rates and earthquake recurrence models to probabilistic seismic hazard estimates, Bull. Seism. Soc. Am. 75, 939-964.

5-2 Ground Modeling

Earthquake motion at the ground surface is strongly affected by subsurface soil structure. The effects of soils on seismic motion are evaluated by numerical simulation. For this purpose, digital ground surface models with 250 m grid cells were constructed based on geological, geotechnical and geophysical information. These ground models were also used in liquefaction potential analysis. The ground modeling was conducted following the flow in Figure 5-2.

(1) Compilation of Boring Logs and PS Logging

The boring logs and PS loggings conducted in this study were compiled along with existing boring data.

(2) Determination of Engineering Seismic Bedrock

Depending on the existing geological map, existing boring, literature, compiled boring logs and PS loggings, fresh Plaisancian blue marl (p1-f) with Vs of 630 m/sec and fresh schist (mi-f) with Vs of 1030 m/sec were adopted as “engineering” seismic bedrock.

(3) Compilation of Laboratory Tests

The laboratory test data collected in this study were compiled along with the collected existing data.

(4) Identification of Soil Classifications

Based on the compiled boring data, PS logging data and laboratory test data, the soils identified in the Study Area were classified for the purpose of engineering geology. The soil layers in each boring log were classified according to this classification.

(5) Smooth Interpolation

The depth of Schist, Plaisancian layer and Astian layer in each 250 m grid cell was estimated with numerical interpolation techniques using these limited points of data.

(6) Surface Soil

The geological map was used to estimate surface soil condition in each 250 m grid cell. Figure 5-3 shows the surface soil distribution.

(7) Setting of Average Soil Properties

The geotechnical and geophysical parameters; i.e. Vs, density, depth, etc., were set for each layer of the 250 m grid model.

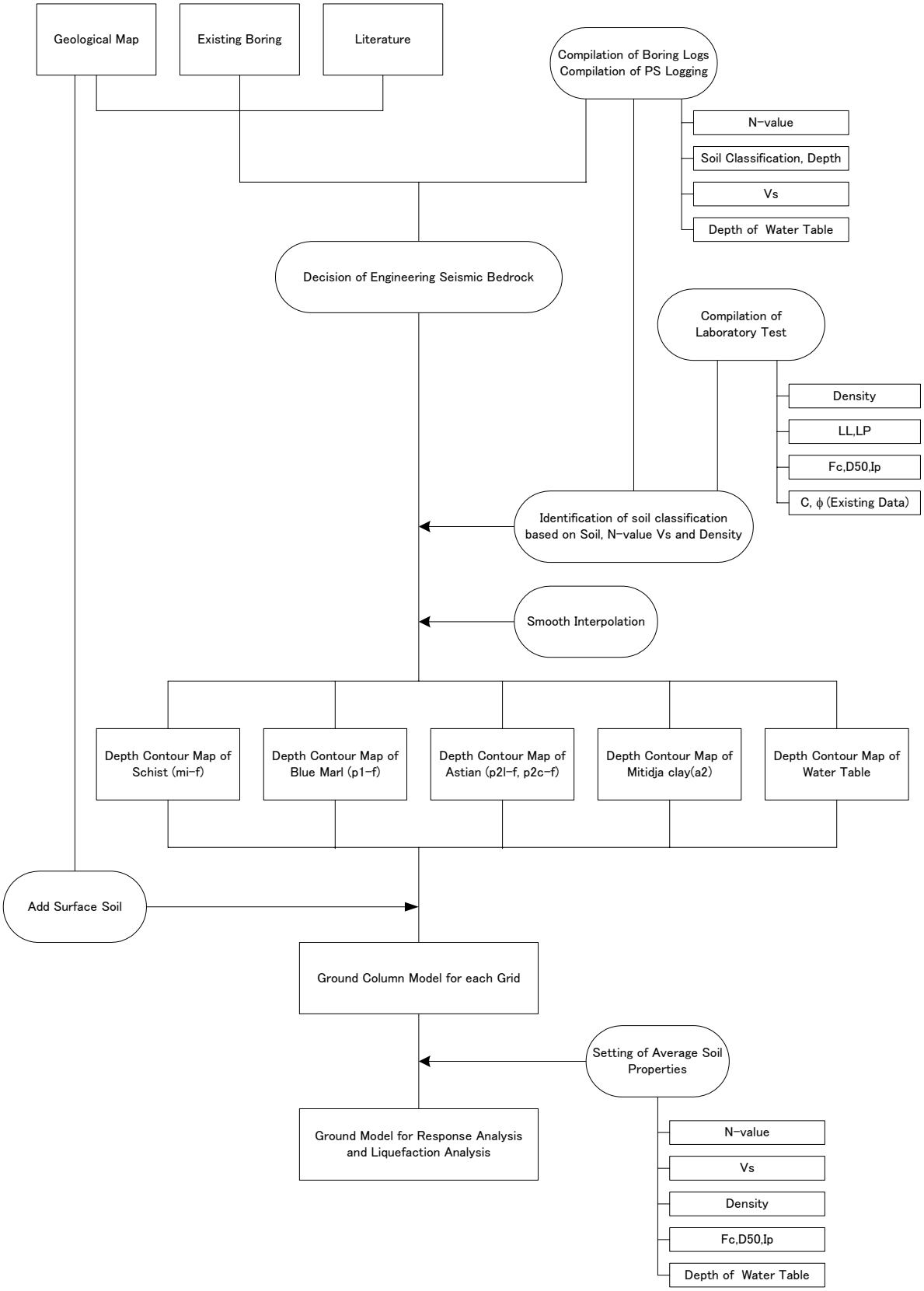

Figure 5-2 Ground Modeling Flowchart

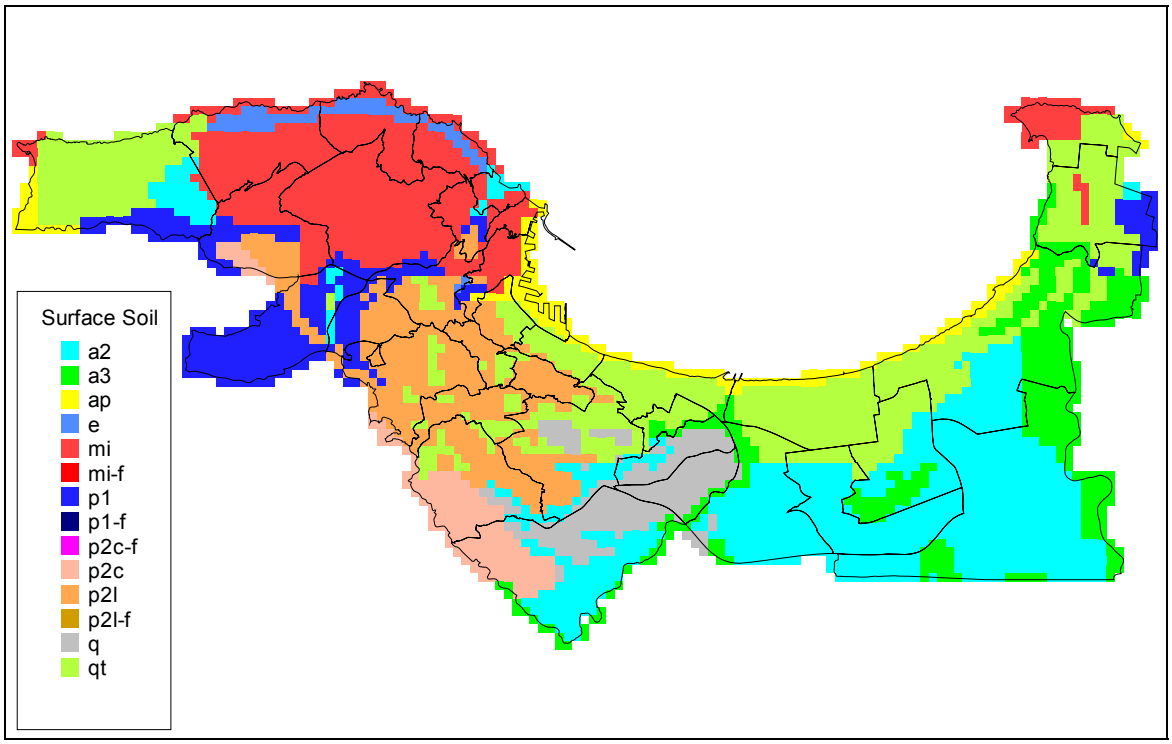

Figure 5-3 Surface Soil

5-3 Estimation of Ground Motion

5-3-1 Bedrock Motion Analysis

Horizontal Peak Ground Accelerations at bedrock, as associated with reference earthquakes, were calculated using appropriate attenuation relationships. The applicability of several preselected attenuation relationships to the Algiers area was evaluated through comparison with the strong motion records observed in the 2003 Boumerdes earthquake. The following formula by Ambraseys et al. (2005) was selected to calculate PGA in study area.

$$\log y = 2.522 - 0.142Mw + (-3.184 + 0.314Mw)\cdot \log\sqrt{d^2 + 7.6^2} + \begin{cases} 0.137 : \text{soft soil} \\ 0.050 : \text{stiff soil} \\ 0.0 \quad : \text{rock} \end{cases} + \begin{cases} 0.062 : \text{thrust} \\ 0.0 : \text{strike - slip} \end{cases}$$

y : PGA(m/sec^2)

Mw : moment magnitude

d : distance to the surface projection of the fault (km)

The source fault models of the six scenario earthquakes are shown in Figure 5-4. For each fault model, the distance from the center of each grid cell to the surface projection of the source faults was measured and the PGA at bedrock was calculated.

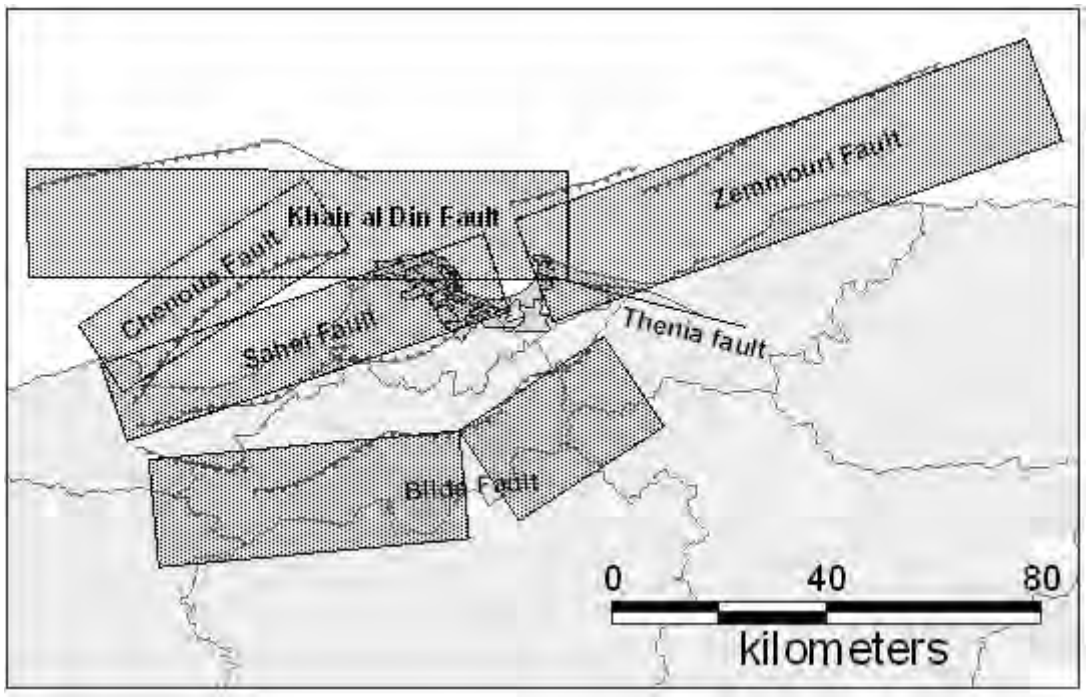

Figure 5-4 Fault Models of Scenario Earthquakes

5-3-2 Subsurface Amplification Analysis

Earthquake motion at the ground surface is strongly affected by subsurface soil structures, especially in the areas covered by quaternary sediments. The effects of soils on seismic motion were evaluated by response analysis based on the 4013 ground models of the 250 m grid. The amplification of subsurface soil over engineering seismic bedrock was estimated by the 1D response analysis code SHAKE.

The response analysis was conducted both in linear and non-linear contexts to check the effect of the non-linear property. As there is no dynamic soil laboratory test to evaluate the non-linear dynamic property of soil in Algeria, the existing non-linear dynamic property of soil used in a seismic microzoning study of the Tokyo, Japan Metropolitan Area was applied after considering the similarities of soil, S-wave velocity and N-value.

The estimated bedrock waves during the 2003 Boumerdes earthquake were used as input motion. The magnitude of the Boumerdes earthquake, Mw=6.9, is comparable to the scenario earthquakes and the distance from source area to the Study Area also does not differ much. Therefore the frequency of the observed seismic waves in Algiers during the Boumerdes earthquake is suitable for input motion of the response analysis.

5-3-3 Evaluation of Earthquake Ground Motion

The PGA value of the ground surface at each grid cell (Figure 5-5) was calculated from bedrock motion and response analysis. The results of linear analysis show slightly larger PGA in the eastern area; however, the difference is small. The results of non-linear analysis are subsequently used as the PGA distribution.

The seismic intensity distribution in the MSK scale (Figure 5-6) was estimated by a newly devised empirical relationship. The seismic intensity and strong motion records collected by CGS during the 1989 Chenoua earthquake, the 1999 Ain Timouchent earthquake and the 2003 Boumerdes earthquake, were collected and a new relationship for Algeria was devised.

[References]

Ambraseys N.N., Douglas J., Sarma S.K. and Smit P.M., 2005, Equations for the Estimation of Strong Ground Motions from Shallow Crustal Earthquakes Using Data from Europe and the Middle East: Horizontal Peak Ground Acceleration and Spectral Acceleration. Bulletin of Earthquake Engineering, 3, pp.1-53.

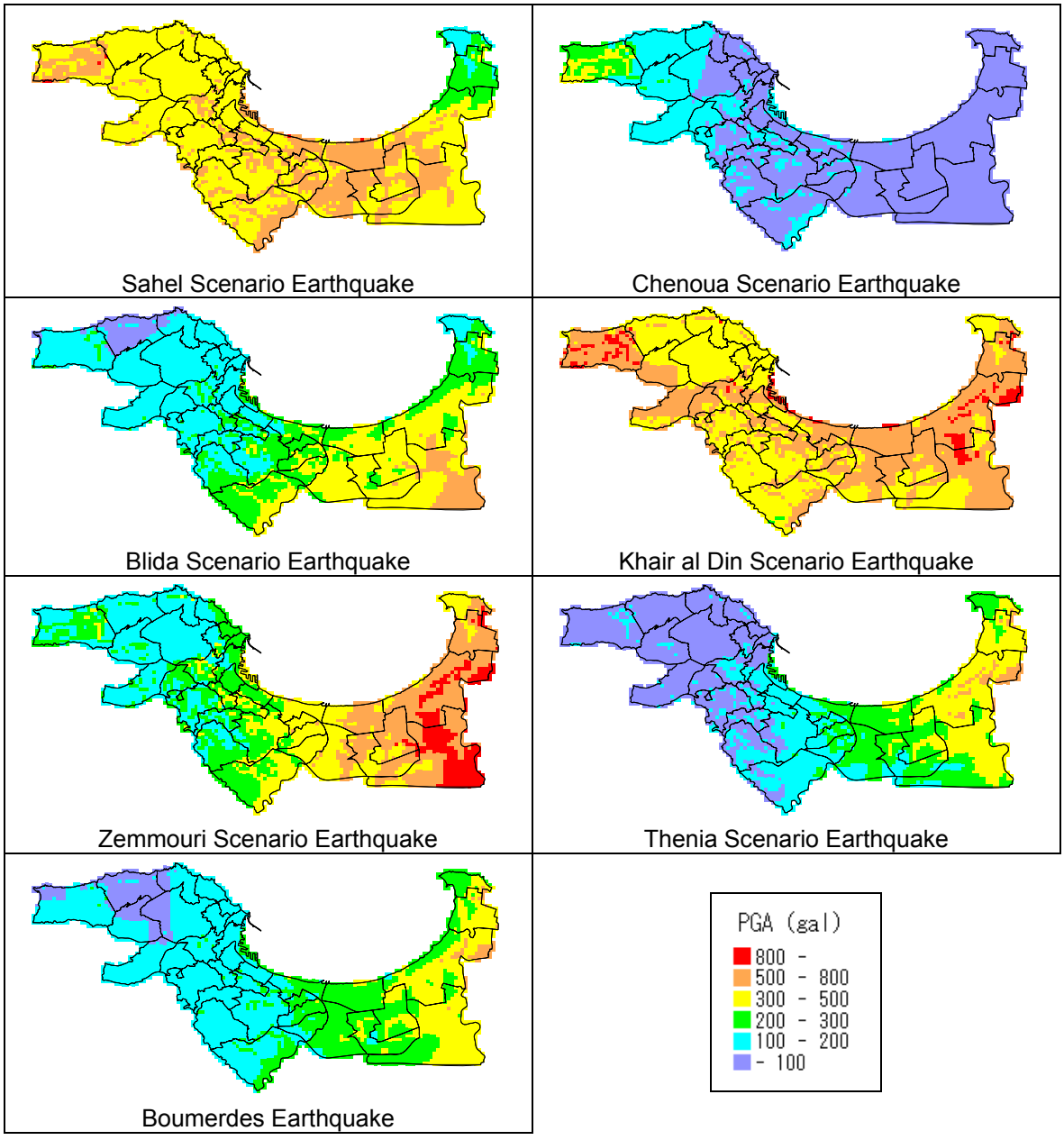

Figure 5-5 Peak Ground Acceleration Distribution at the Ground Surface

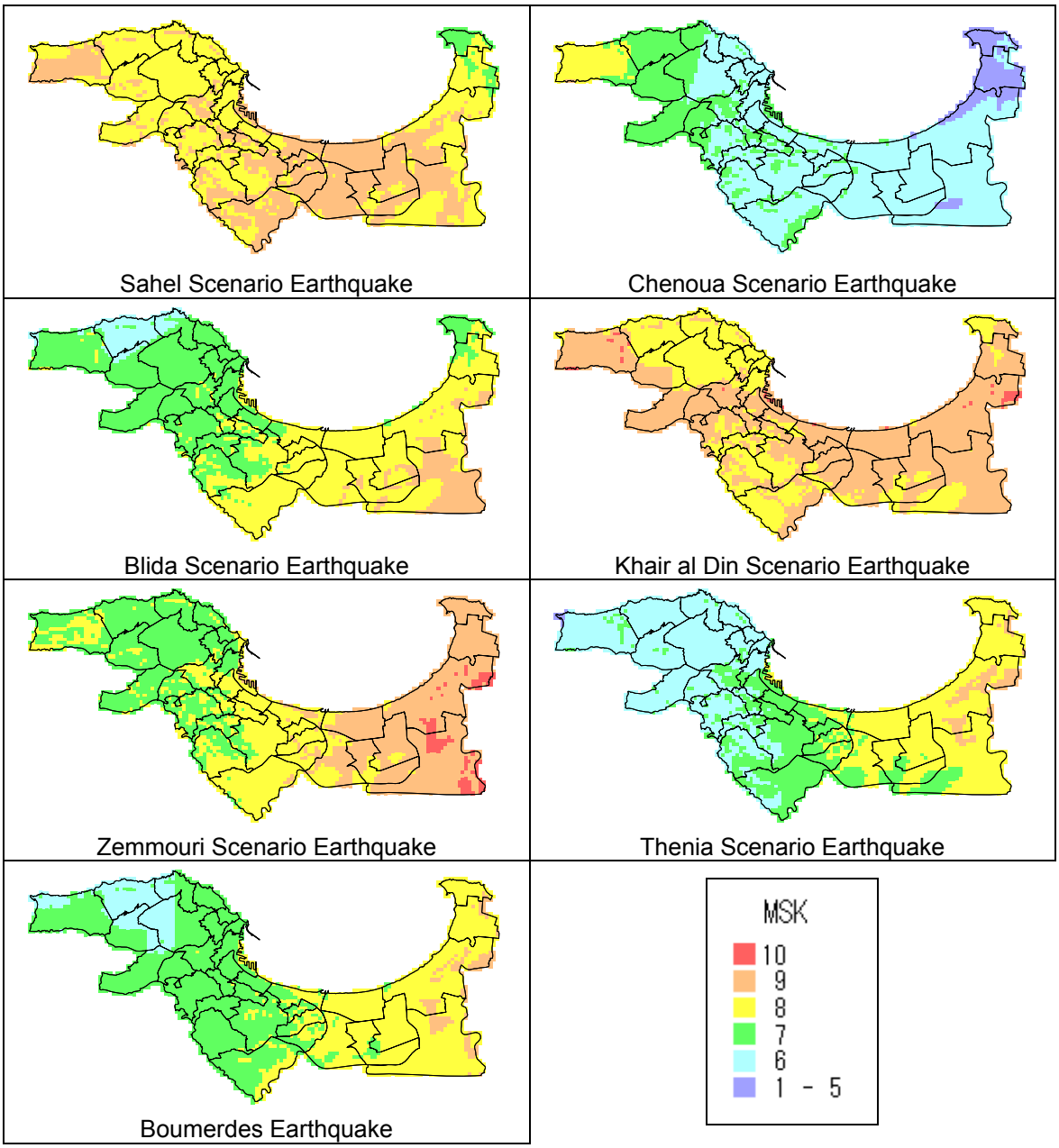

Figure 5-6 Seismic Intensity Distribution in the MSK Scale

5-4 Estimation of Liquefaction Potential

5-4-1 Methodology

The F_L method (Japan Road Association, 2002) was adopted to estimate the liquefaction potential of the deposits at each depth. The approach of this F_L method to the assessment of liquefaction potential consists of the following steps:

1) Estimation of the liquefaction resistance of soils in a deposit (R);
2) Estimation of the shear stress likely to be induced in the soil deposit during an earthquake (L);

3) Estimation of the liquefaction potential (F_L) of the deposit, based on 1) and 2).

For the seismic microzoning purpose, it is important to estimate its effect on the ground surface or structures rather than the occurrence of liquefaction itself in the deposit. For this purpose, the liquefaction potential index P_L by Iwasaki et al. (1982) was adopted in this study.

5-4-2 Preconditions for the Analysis

(1) Soil Layers Studied and their Geotechnical Properties

The soils that require a liquefaction potential study are basically recent deposits. Liquefaction is not expected if Fc is more than 35% and Ip is more than 15%. In this study area, “ap”, “e”, “a3”, “q” and “qt” meet this criteria.

(2) Groundwater Level

Several groundwater levels, which were observed by supplemental investigation and collected from existing boring records show obvious discrepancies with records of other points. This may be because the other records were for the water level of a deeper aquifer rather than the surface aquifer. The groundwater level required in the analysis of liquefaction potential is the shallowest one; therefore the groundwater level for the ground model was determined by observed data and engineering judgment.

5-4-3 Liquefaction Potential

Liquefaction potential was evaluated using the P_L value (Table 5-2). The results are summarized in Figure 5-7.

Table 5-2 Criterion for Evaluation of Liquefaction Potential

Liquefaction Potential	Criterion	Explanation
High	$15 < P_L$	Ground improvement is indispensable
Relatively High	$5 < P_L \leq 15$	Ground improvement is required Investigation of important structures is indispensable
Relatively Low	$0 < P_L \leq 5$	Investigation of important structures is required
Low	$P_L = 0$	Liquefaction prone area

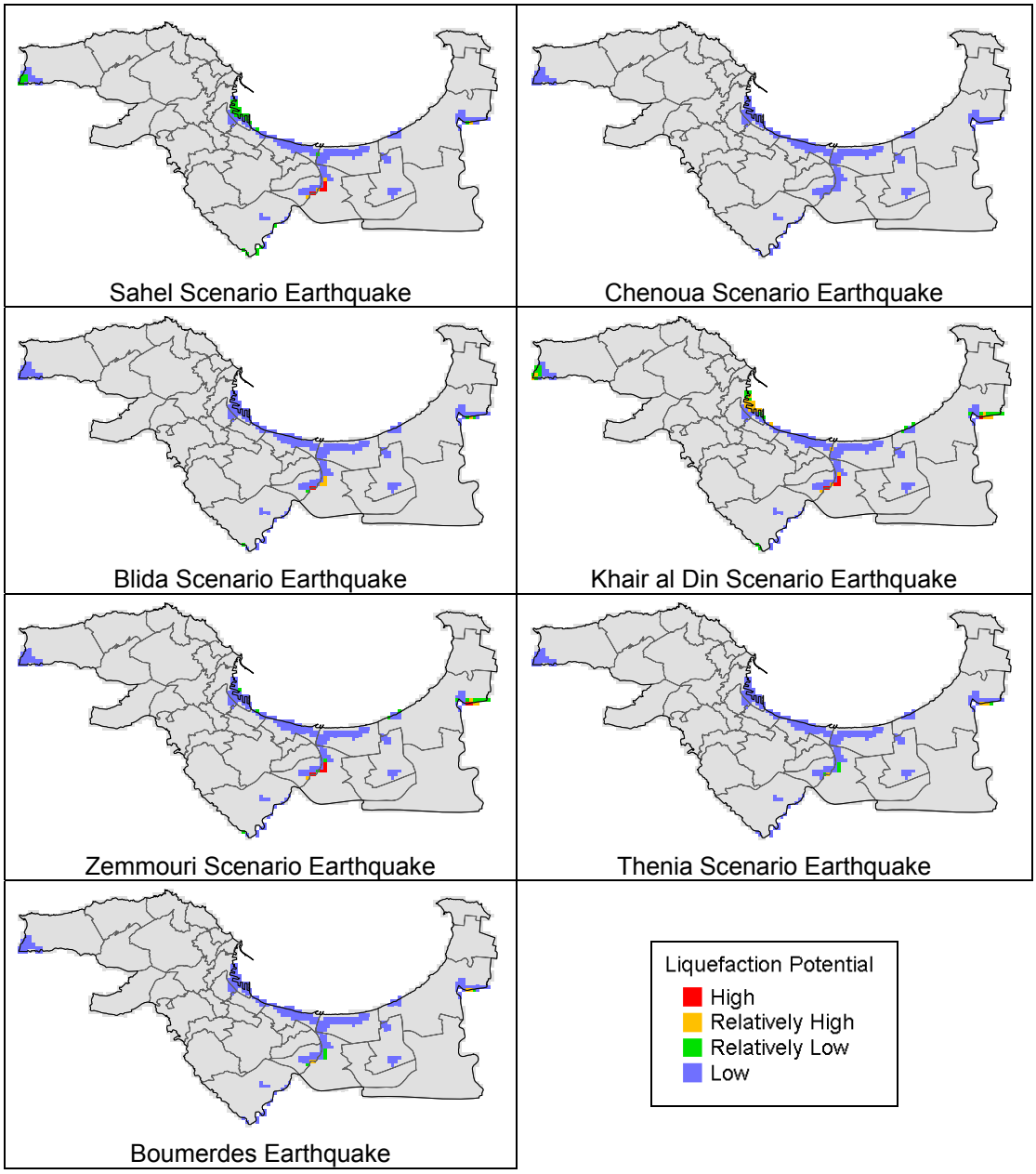

Figure 5-7 Liquefaction Potential Distribution

[References]

Iwasaki, T., Tokida, K., Tatsuoka, F., Watanabe, S., Yasuda, S. and Sato, H., 1982, Microzonation for Soil Liquefaction Potential Using Simplified Methods, Proc., 3rd Int. Conf. on Microzonation, Seattle, Vol.3, pp1319-1330.

Japan Road Association (2002). Specifications for Highway Bridges, Part V Earthquake Resistant Design.

5-5 Estimation of Slope Stability

5-5-1 Methodology

Two types of slope are generally found in the study area, these being steep and gentle. The type is dependant on the geology; Schist (mi) and Calcareous sandstone (p2l) generally form steep slopes; other formations form gentle slopes. The former is expected to result from a collapse and the latter from a land slide. Therefore, 'mi' and 'p2l' were assessed based by Wilson et al. (1979) while the other was assessed by Ansal and Siyahi (1994).

5-5-2 Preconditions for the Analysis

(1) Critical Acceleration

Using the values of c and ϕ for each layer, the critical acceleration against the slope-inclination was calculated using Wilson's method and Ansal and Siyahi's method.

(2) Distribution of slope angles

The slope angle was calculated at 5 m intervals based on the DEM data, which was produced by INCT, and the elevation data based on the 1/10,000 topographical map.

(3) Correction of the slope angle

In using the DEM data for slope analysis, limitations to the accuracy based on the sampling interval should be considered. The numerical parameter study was conducted for many slopes with various heights and widths and the relationship between actual slope angle and slope angle based on the DEM was studied. Based on this study, a correction formula was developed.

Comparing the PGA value for each scenario earthquake and 'Critical acceleration', the stability category of stable ($Fs \geq 1$) or unstable ($Fs < 1$) was judged at each 5 m DEM data point. The slope failure potential of each 250 m grid cell was evaluated based on the ratio of unstable DEM data points in each grid cell.

5-5-3 Evaluation of Slope Stability

Figure 5-8 shows the slope failure potential using the method described above. In this figure, the Boumerdes earthquake was evaluated as having very little area with potential for slope failure. This is consistent with the following description of this earthquake hazard: 'During a post-earthquake reconnaissance, only a few minor landslides and road cut failures were observed. No major landslides were observed.' (EERI, 2003).

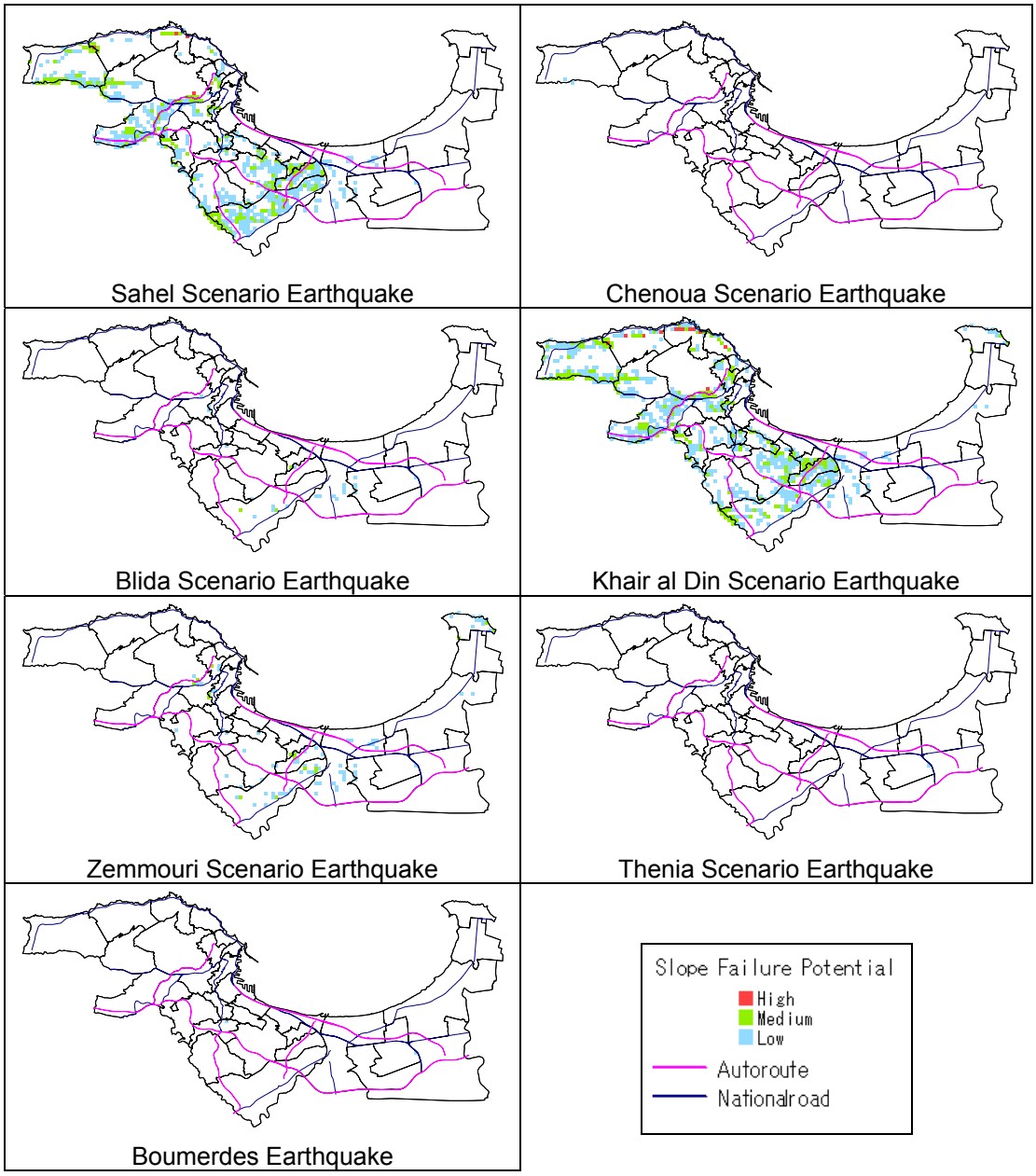

Figure 5-8 Slope Failure Potential Distribution

5-5-4 Slope Site Inspection

As the next step, individual slope inspection is recommended for grid cells with a high potential for slope failure based on the grid analysis. The main aims of the proposed site slope inspections were to:

- decide the extent of the slope.
- evaluate the slope stability.
- determine the kind and amount of infrastructure that may be affected by a slope failure.

The slope site inspection was carried out by a study team made up of the CGS Team and the JICA Study Team. The slopes inspected are shown in Figure 5-9. Table 5-3 is the summary of the inspections.

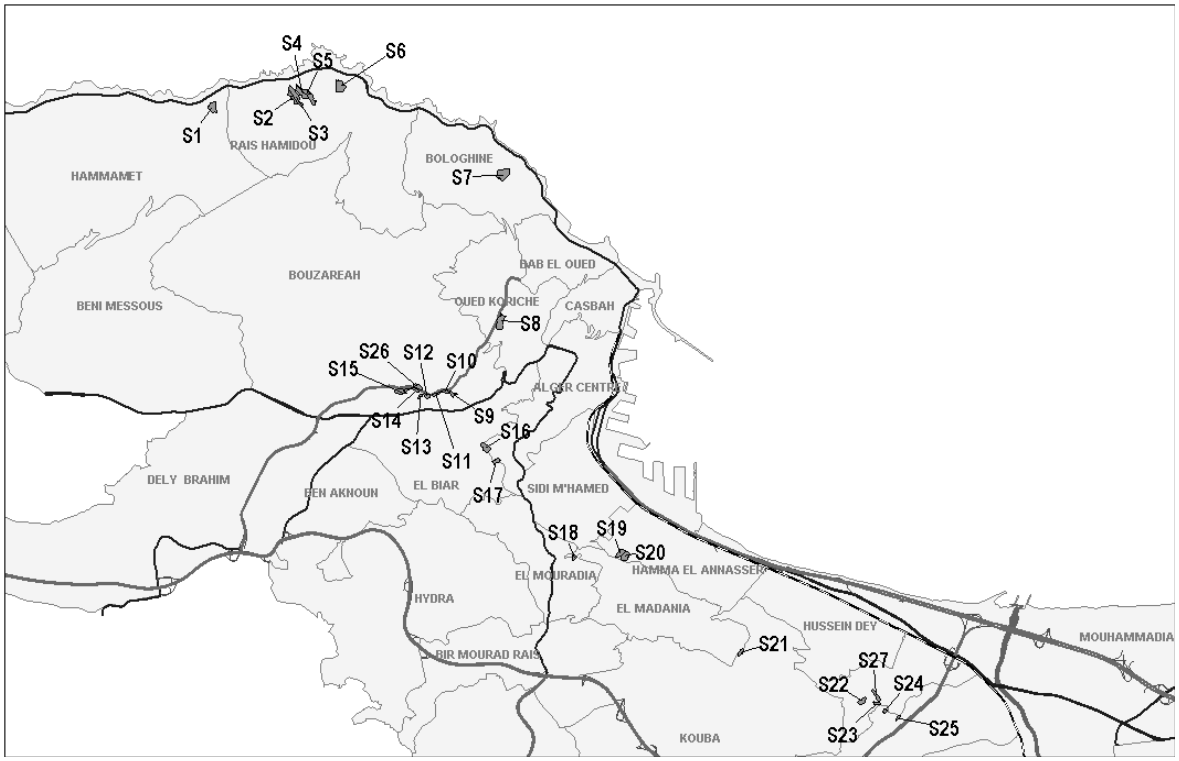

Figure 5-9 Locations of Inspected Slopes

Table 5-3 Summary of Site Slope Inspections

Location ID	Total Score	Slope Evaluation with Seismic Intensity				
		X<	IX - X	VIII - IX	VII - VIII	VI - VII
S1	18	A	A	B	C	C
S2	23	A	A	A	B	C
S3	23	A	A	A	B	C
S4	27	A	A	A	B	C
S5	21	A	A	B	C	C
S6	23	A	A	A	B	C
S7	23	A	A	A	B	C
S8	24	A	A	A	B	C
S9	18	A	A	B	C	C
S10	17	A	A	B	C	C
S11	20	A	A	B	C	C
S12	21	A	A	B	C	C
S13	17	A	A	B	C	C
S14	21	A	A	B	C	C
S15	27	A	A	A	B	C
S16	24	A	A	A	B	C
S17	24	A	A	A	B	C
S18	24	A	A	A	B	C
S19	29	A	A	A	B	C
S20	26	A	A	A	B	C
S21	27	A	A	A	B	C
S22	20	A	A	B	C	C
S23	21	A	A	B	C	C
S24	29	A	A	A	B	C
S25	11	A	B	C	C	C
S26	21	A	A	B	C	C
S27	20	A	A	B	C	C

[References]

Ansal, A and B.G. Siyahi, 1994, Microzonation for landslides during earthquakes, 2nd Int. Conf. on Earthquake Resistant Construction & Design, Savidis(ed), Balkema, 151-157.

EERI, 2003, The Boumerdes, Algeria, Earthquake of May 21, 2003, EERI Learning from Earthquakes Reconnaissance Report.

Wilson, R.C., G.F. Wieczorek, E.L. Horp, 1979, Development of Criteria for regional Mapping of Seismic Slope Stability, Abstract, 1979 Annual Meeting of the Geological Society of America.

Chapter 6. Damage Estimation

6-1 Damage of Buildings

The European Macro-seismic Scale, EMS (former MSK) was applied for building damage estimation.

6-1-1 Building Categories

According to the result of a building inventory survey, a study of the seismic codes, and an investigation of damage ratio by earthquakes in the study area, following 8-categories were used;

1. Brick Masonry at Casbah
2. Stone and Brick Masonry
3. RC Frames with Pre-code (non-engineered)
4. RC Frames with Low-code (RPA81,83&88)
5. RC Frames with Moderate-code (RPA99)
6. RC Frames with High-code (RPA99ver.2003)
7. RC Shear Walls and a Mixed Frames
8. Steel

The ratio of building type at each commune is shown in Table 6-1.

Table 6-1 Ratio of Building Type at each Commune

Type of Structure	ID	1601	1602	1603	1604	1605	1606	1607	1608	1609	1610	1611	1612
	COMMUNE	ALGER CENTER	SIDI M HAMED	EL MADANIA	HAMMA EL ANNASSER	BAB EL OUED	BOLOGHINE	CASBAH	OUED KORICHE	BIR MOURAD RAIS	EL BIAR	BOUZAREAH	BIRKHADEM
Old Brick Masonry at Casbah	%	0.0	0.0	0.0	0.0	0.0	0.0	35.7	0.0	0.0	0.0	0.0	0.0
Stone and Brick Masonry	%	77.4	66.0	72.4	12.5	75.5	37.5	64.3	46.7	25.0	33.3	15.8	31.3
RC Frame Pre-code	%	20.8	30.0	13.8	75.0	18.4	50.0	0.0	53.3	41.7	56.7	68.4	65.6
RC Frame Low-code	%	0.0	4.0	3.4	12.5	4.1	8.3	0.0	0.0	4.2	6.7	2.6	0.0
Steel	%	0.0	0.0	0.0	0.0	2.0	4.2	0.0	0.0	0.0	0.0	0.0	0.0
RC Wall	%	0.0	0.0	10.3	0.0	0.0	0.0	0.0	0.0	25.0	3.3	10.5	3.1
RC Frame Medium-code	%	1.9	0.0	0.0	0.0	0.0	0.0	0.0	0.0	4.2	0.0	2.6	0.0
RC Frame High-code	%	0.0	0.0	0.0	0.0	0.0	0.0	0.0	0.0	0.0	0.0	0.0	0.0

Type of Structure	ID	1613	1615	1616	1617	1618	1619	1620	1621	1622	1623	1624	1625
	COMMUNE	EL HARRACH	OUED SMAR	BOUROUBA	HUSSEIN DEY	KOUBA	BACH DJARAH	DAR EL BEIDA	BAB EZZOUAR	BEN AKNOUN	DELY BRAHIM	HAMMAMET	RAIS HAMIDOU
Old Brick Masonry at Casbah	%	0.0	0.0	0.0	0.0	0.0	0.0	0.0	0.0	0.0	0.0	0.0	0.0
Stone and Brick Masonry	%	55.6	0.0	25.6	46.4	25.0	18.0	0.0	3.9	9.1	0.0	18.2	41.7
RC Frame Pre-code	%	37.0	91.7	62.8	39.3	35.7	48.0	44.0	21.6	54.5	82.4	81.8	41.7
RC Frame Low-code	%	0.0	8.3	4.7	3.6	10.7	12.0	32.0	15.7	0.0	5.9	0.0	0.0
Steel	%	0.0	0.0	0.0	3.6	1.8	0.0	8.0	0.0	0.0	0.0	0.0	0.0
RC Wall	%	3.7	0.0	2.3	3.6	26.8	22.0	16.0	49.0	36.4	0.0	0.0	16.7
RC Frame Medium-code	%	3.7	0.0	4.7	0.0	0.0	0.0	0.0	7.8	0.0	0.0	0.0	0.0
RC Frame High-code	%	0.0	0.0	0.0	3.6	0.0	0.0	0.0	2.0	0.0	11.8	0.0	0.0

Type of Structure	ID	1626	1627	1628	1629	1630	1631	1632	1639	1640	1644	Total
	COMMUNE	DJASR KACENTINA	BELOUIDAD	HYDRA	MOHAMMADIA	BORDJ EL KIFFAN	EL MAGHARIA	BENI MESSOUS	BORDJ EL BAHRI	EL MARSA	AIN BENIAN	
Old Brick Masonry at Casbah	%	0.0	0.0	0.0	0.0	0.0	0.0	0.0	0.0	0.0	0.0	1.0
Stone and Brick Masonry	%	10.9	84.8	0.0	13.0	15.3	11.8	10.0	13.3	20.0	24.1	33.6
RC Frame Pre-code	%	37.0	6.1	75.0	34.8	18.6	58.8	50.0	66.7	80.0	44.8	40.6
RC Frame Low-code	%	10.9	0.0	0.0	30.4	49.2	5.9	30.0	13.3	0.0	24.1	10.0
Steel	%	2.2	0.0	0.0	0.0	3.4	0.0	0.0	0.0	0.0	0.0	0.9
RC Wall	%	39.1	9.1	20.0	21.7	3.4	23.5	10.0	6.7	0.0	6.9	11.9
RC Frame Medium-code	%	0.0	0.0	5.0	0.0	10.2	0.0	0.0	0.0	0.0	0.0	1.7
RC Frame High-code	%	0.0	0.0	0.0	0.0	0.0	0.0	0.0	0.0	0.0	0.0	0.4

6-1-2 Building Damage of the 1980 El Asnam and 2003 Boumerdes Earthquakes

CTC surveyed damages of approximately 10,000 buildings caused by the 1980 EL Asnam Earthquake using a "Damage Evaluation Form", and damages were classified into 5 damage grades.

CGS and CTC executed a damage survey by the 2003 Boumerdes Earthquake in Wilaya Boumerdes and Algiers. Refer to Chapter 4-1-2 for detail.

6-1-3 Damage Function of Buildings

(1) General

The damage survey results for four structural types by the 2003 Boumerdes earthquake for following three communes inside the study area were provided by CGS;

(1621) Beb Ezzour, (1630) Bordj El Kiffan, (1639) Bordj El Bahri

However these communes are located at east side of Wilaya Algiers, and the estimated EMS (former MSK) seismic intensity was around 8, and there was no clear difference of the intensity among three communes. As a result, it was not possible to produce a damage function of buildings from the damage survey data only. It has been proposed to introduce an idea of a distribution of seismic index of structure, Is, for each structural type and to combine with the surveyed damage ratio.

(2) Seismic Intensity and Surveyed Damage Ratio

The EMS seismic intensity related to PGA has been used for the horizontal axis of 'Damage Function'. Refer to Chapter 5 for the Estimation of Ground Motion. The estimated seismic intensity is shown in Table 6-2. By the engineering judgment, reduced values of surveyed damage ratio were used at the average seismic intensity 8.0, considering a wide range of the estimated seismic intensity.

Table 6-2 Estimated Seismic Intensity by Boumerdes Earthquake

Name of Commune	Estimated Seismic Intensity	Ratio of Surveyed Buildings
BAB EZZOUAR	average 7.9 (min.7.4~max.8.5)	14 %
BORDJ EL KIFFAN	average 8.2 (min.7.4~max.9.0)	22 %
BORDJ EL BAHRI	average 8.0 (min.7.8~max.8.8)	26 %

(3) A Methodology Incorporating Seismic Index of Structure, Is,

The damage function for RC moment frame structures with Pre-code (non-engineered) was estimated as shown in Figure 6-1.

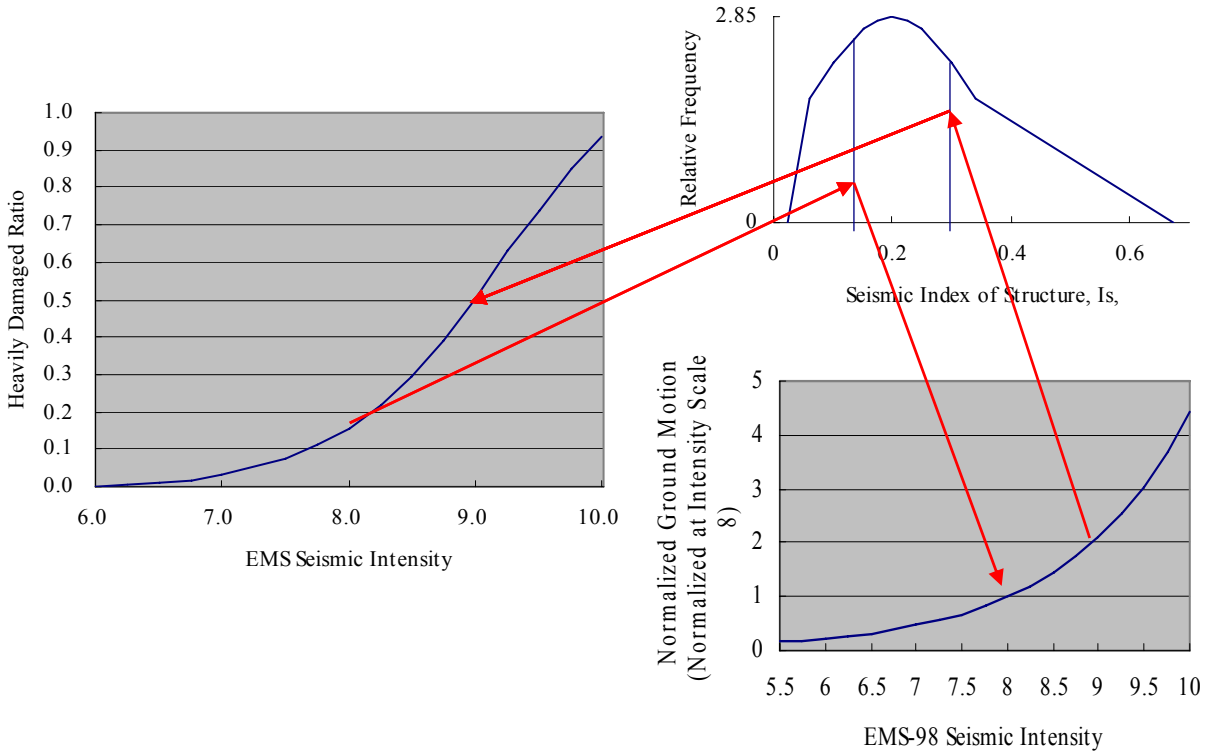

Figure 6-1 Seismic Index of Structure, Seismic Intensity and Heavily Damaged Ratio

Supposed Seismic Index of structure for each structural type is shown in Figure 6-2.

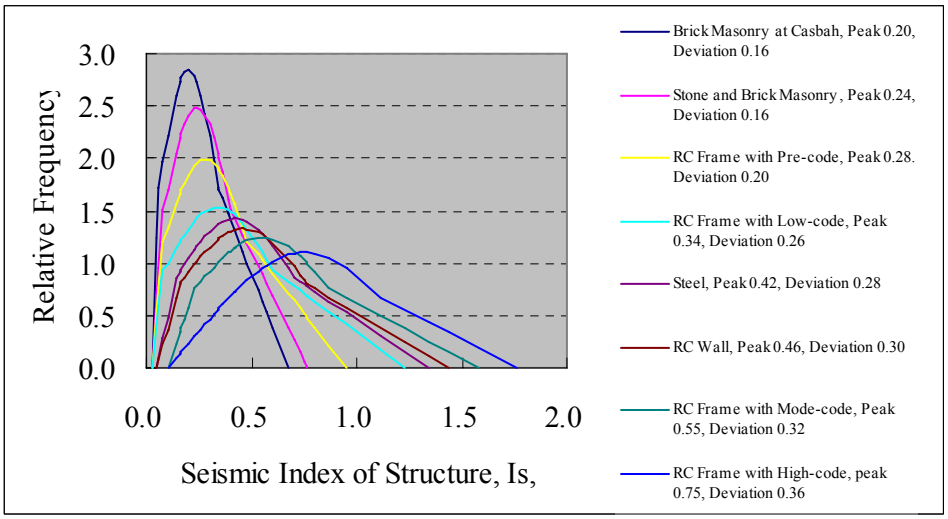

Figure 6-2 Supposed Seismic Index of Structure for each Structural Type

(4) Damage Function

Similar estimation was done with respect to total eight structural types as shown in Figure 6-3.

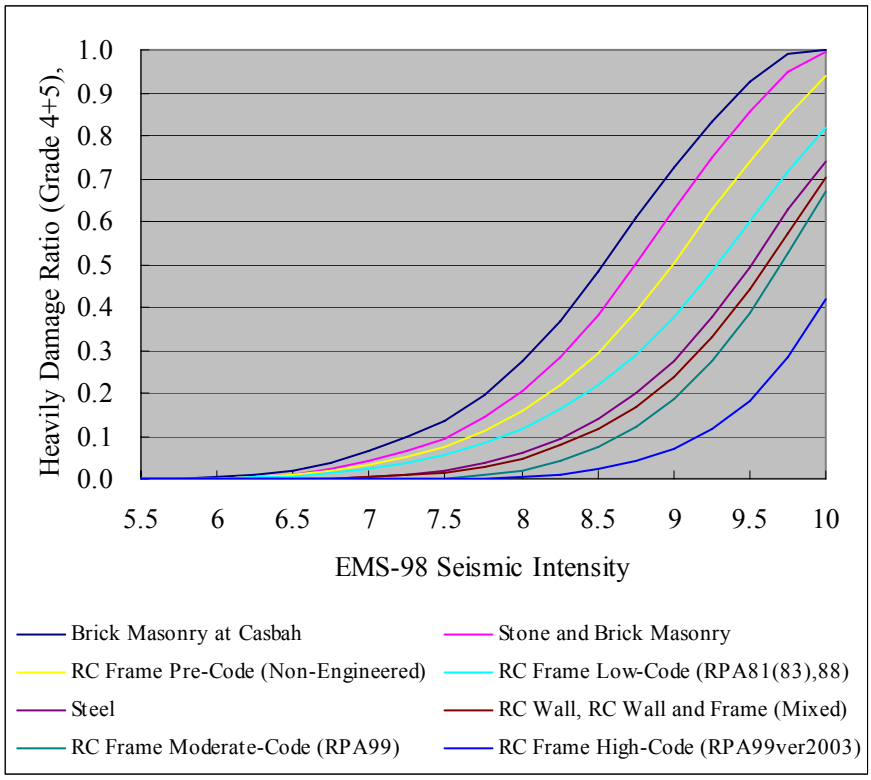

Figure 6-3 Damage Function of Buildings

(5) Calibration

The heavily damage ratio at seismic intensity 8.0 was reduced to a range of 80% ~ 60% of the surveyed ratio by the engineering judgment as shown in Figure 6-4.

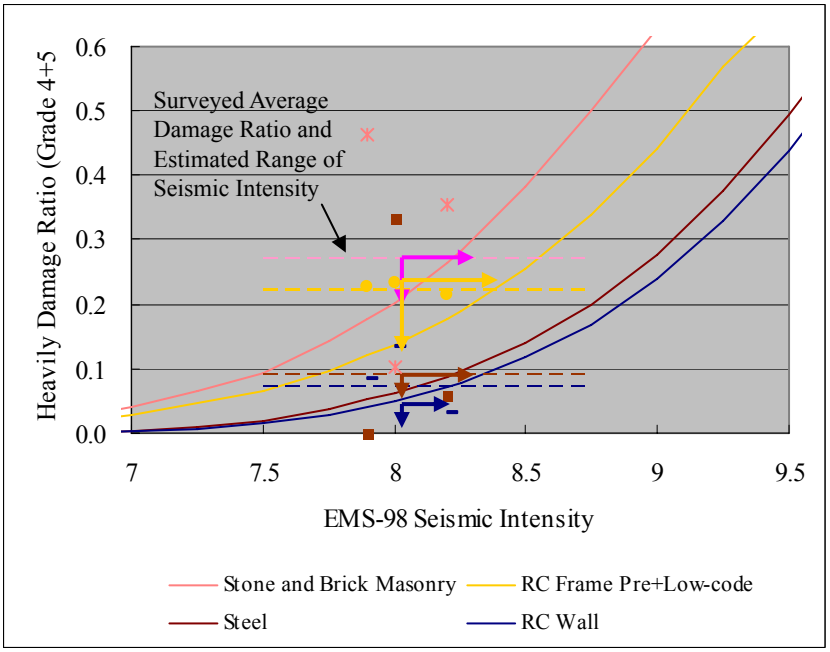

Figure 6-4 Surveyed Average Damage Ratio, Estimated Range of Seismic Intensity by Boumerdes Earthquake and Damage Function

6-1-4 Estimated Damage

(1) Inventory estimation

The building inventory was estimated based on the GIS data and inventory survey. First the buildings were attributed to the 250m grid sector in which the center of the polygon was located. The ratios of building types in each commune were estimated from the inventory survey. The ratios of building types in the commune that contains the grid sector were used to estimate the number of buildings of each class in each grid sector.

(2) Damage estimation

Damage to buildings was estimated for two scenario earthquakes. The estimated number of heavily damaged buildings is shown in Table 6-3. In Table 6-3, the degree of damage from the 2003 Boumerdes earthquake was reproduced with this methodology and is also included. The distribution of heavily damaged buildings is shown in Figure 6-5.

Table 6-3 Building Damage

ID	Commune Name	Inventory		Khair al Din Scenario eq.				Zemmouri Scenario eq.				2003 Boumerdes eq.			
		Building	Housing Unit	Building		Housing Unit		Building		Housing Unit		Building		Housing Unit	
1601	ALGER CENTRE	3,396	16,219	1,395	41%	6,662	41%	379	11%	1,808	11%	98	3%	468	3%
1602	SIDI M'HAMED	2,206	13,863	922	42%	5,795	42%	235	11%	1,475	11%	65	3%	411	3%
1603	EL MADANIA	3,124	8,788	1,435	46%	4,037	46%	492	16%	1,384	16%	148	5%	417	5%
1604	HAMMA EL ANNASSER	2,169	8,594	834	38%	3,305	38%	265	12%	1,049	12%	79	4%	312	4%
1605	BAB EL OUED	1,884	13,184	616	33%	4,311	33%	155	8%	1,081	8%	28	1%	198	1%
1606	BOLOGHINE	2,933	6,643	899	31%	2,037	31%	212	7%	479	7%	39	1%	89	1%
1607	CASBAH	2,739	10,175	1,067	39%	3,963	39%	282	10%	1,049	10%	57	2%	211	2%
1608	OUED KORICHE	2,585	8,823	978	38%	3,337	38%	246	10%	838	10%	63	2%	216	2%
1609	BIR MOURAD RAIS	4,696	6,927	1,249	27%	1,842	27%	331	7%	488	7%	92	2%	135	2%
1610	EL BIAR	7,408	8,616	3,393	46%	3,946	46%	820	11%	953	11%	249	3%	290	3%
1611	BOUZAREAH	9,804	11,098	2,633	27%	2,980	27%	454	5%	514	5%	80	1%	91	1%
1612	BIRKHADEM	6,459	8,455	1,852	29%	2,424	29%	617	10%	807	10%	187	3%	244	3%
1613	EL HARRACH	4,560	7,296	2,076	46%	3,321	46%	1,555	34%	2,487	34%	499	11%	799	11%
1615	OUED SMAR	3,455	3,092	1,339	39%	1,199	39%	1,352	39%	1,210	39%	411	12%	368	12%
1616	BOUROUBA	4,808	9,385	1,892	39%	3,692	39%	1,259	26%	2,457	26%	431	9%	841	9%
1617	HUSSEIN DEY	4,630	8,015	2,155	47%	3,730	47%	1,024	22%	1,772	22%	329	7%	569	7%
1618	KOUBA	8,940	15,913	2,884	32%	5,133	32%	1,195	13%	2,127	13%	355	4%	632	4%
1619	BACH DJERAH	6,041	15,048	1,895	31%	4,720	31%	1,119	19%	2,787	19%	378	6%	941	6%
1620	DAR EL BEIDA	8,094	6,095	2,941	36%	2,215	36%	3,848	48%	2,897	48%	1,336	17%	1,006	17%
1621	BAB EZZOUAR	5,138	13,544	1,490	29%	3,928	29%	1,531	30%	4,036	30%	418	8%	1,103	8%
1622	BEN AKNOUN	3,299	3,391	1,009	31%	1,037	31%	166	5%	171	5%	42	1%	43	1%
1623	DELY BRAHIM	3,813	4,526	1,309	34%	1,554	34%	198	5%	235	5%	51	1%	60	1%
1624	HAMMAMET	2,223	3,283	687	31%	1,015	31%	98	4%	145	4%	15	1%	23	1%
1625	RAIS HAMIDOU	3,364	3,169	1,047	31%	987	31%	200	6%	188	6%	35	1%	33	1%
1626	DJASR KACENTINA	3,458	12,639	785	23%	2,870	23%	424	12%	1,549	12%	132	4%	484	4%
1627	EL MOURADIA	3,277	5,017	1,675	51%	2,565	51%	512	16%	783	16%	157	5%	241	5%
1628	HYDRA	6,980	6,080	1,967	28%	1,714	28%	417	6%	363	6%	111	2%	97	2%
1629	MOHAMMADIA	4,321	6,749	1,671	39%	2,610	39%	1,304	30%	2,036	30%	369	9%	576	9%
1630	BORDJ EL KIFFAN	10,915	14,375	4,637	42%	6,107	42%	4,911	45%	6,468	45%	1,822	17%	2,400	17%
1631	EL MAGHARIA	2,643	4,559	974	37%	1,680	37%	493	19%	851	19%	153	6%	264	6%
1632	BENI MESSOUS	2,254	2,630	821	36%	958	36%	125	6%	146	6%	33	1%	38	1%
1639	BORDJ EL BAHRI	4,724	4,030	1,799	38%	1,535	38%	2,022	43%	1,724	43%	738	16%	629	16%
1640	EL MARSA	1,330	1,366	504	38%	518	38%	556	42%	571	42%	217	16%	223	16%
1644	AIN BENIAN	6,362	8,252	2,986	47%	3,873	47%	385	6%	499	6%	108	2%	140	2%
Total		154,032	279,838	55,817	36%	101,600	36%	29,176	19%	47,430	17%	9,327	6%	14,592	5%

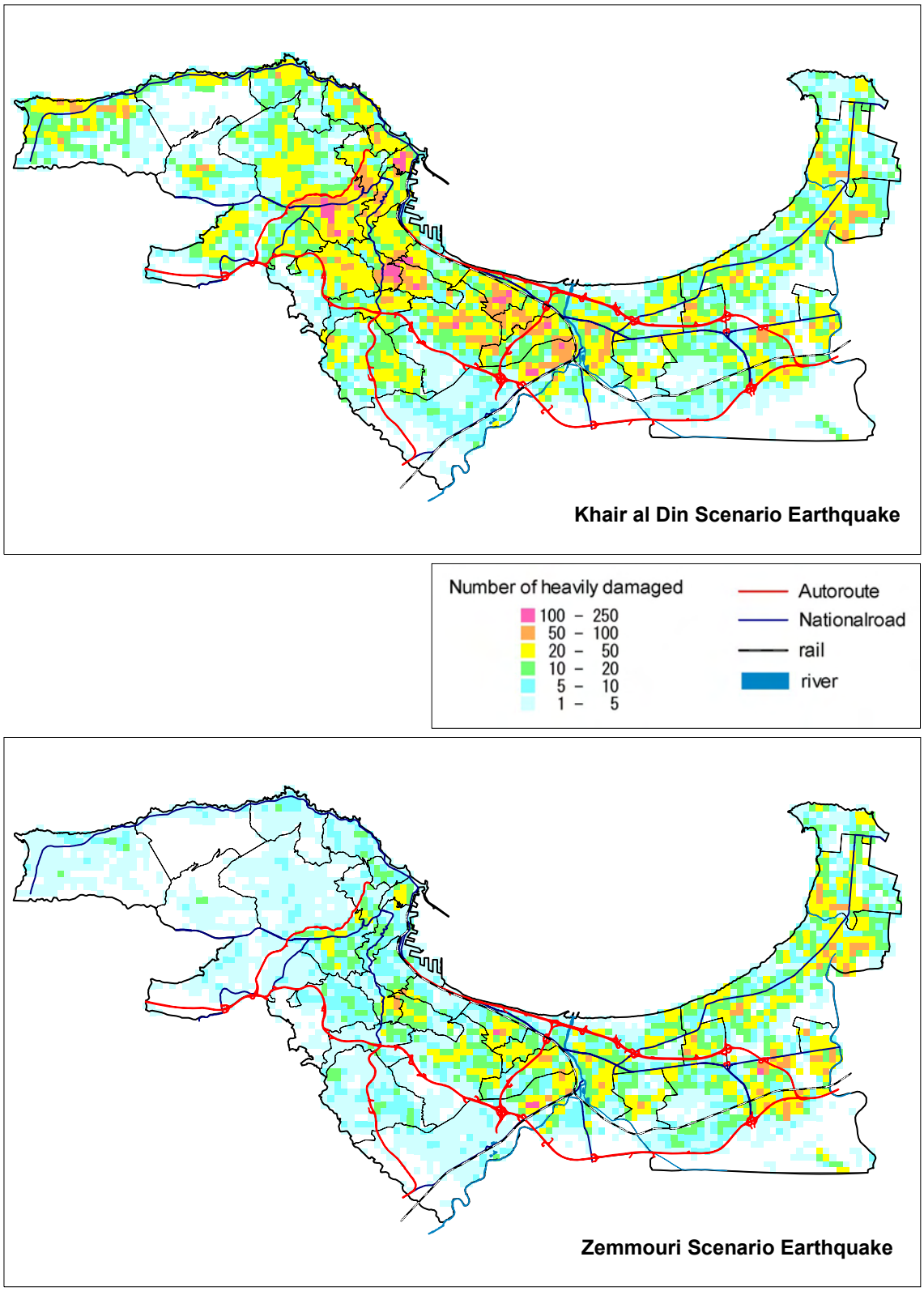

Figure 6-5 Number of Heavily Damaged Buildings

6-2 Human Casualties

6-2-1 Methodology

(1) Damage Data from Past Earthquakes

The number of human casualties and damaged buildings as a result of recent earthquake disasters in Algeria were collected from various documents. The number of damaged dwelling units is a better indicator than that of damaged buildings when estimating human casualties.

(2) Analysis Unit

The human casualties are to be estimated by commune in this Study, therefore the commune is the desirable unit in the damage function analysis. Also the damage function depends on local conditions, e.g. building density, building structure, and rescue system, so the damage data in the target study area is preferable for damage function analysis.

(3) Formulation of the Damage Function

The number of heavily damaged dwelling units was used as the indicator to estimate the number killed. The relationship between the number killed and the number of heavily damaged dwelling units is shown in Figure 6-6. The estimated number of casualties calculated by the damage function in Figure 6-6 has a high degree of uncertainty and the actual outcome in the event of a real earthquake could lie anywhere from half to double the number estimated in this function.

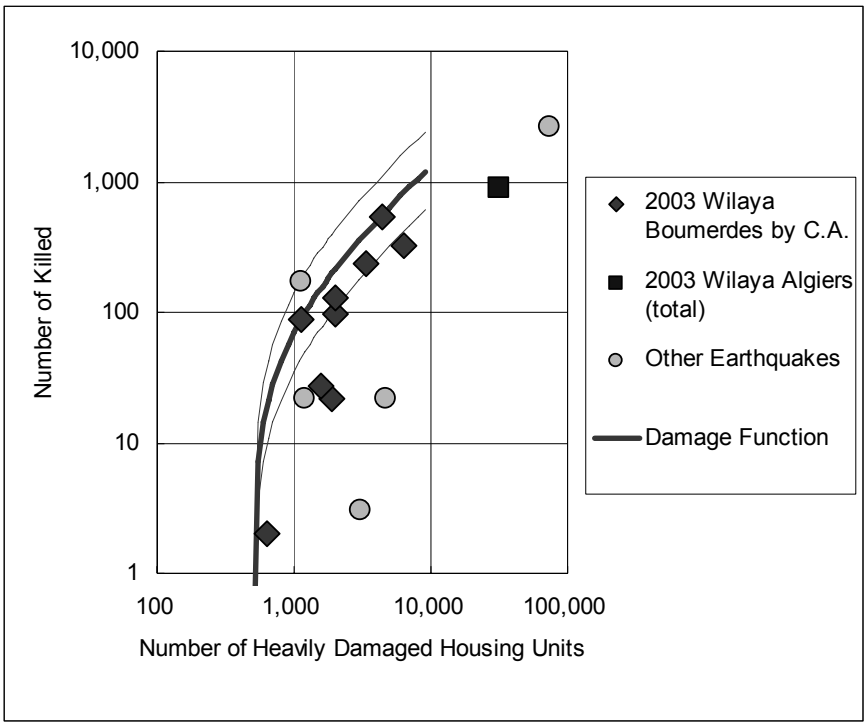

Figure 6-6 Damage Function to Estimate the Number Killed

6-2-2 Damage Estimation

In the estimation, the event is assumed to occur in the evening because the damage function was mainly derived from the 2003 Boumerdes earthquake damages. The estimated number of human casualties and number of homeless people are shown in Table 6-4. The number of homeless people is the people who were previously living in the heavily damaged buildings. In Table 6-4, the damage caused by the 2003 Boumerdes earthquake as reproduced using this methodology is also included. The distribution of the death toll for each commune is shown in Figure 6-7.

Table 6-4 Human Casualties

ID	Commune Name	Population (x1,000)	Khair al Din Scenario eq.			Zemmouri Scenario eq.			2003 Boumerdes eq.		
			Killed (x1,000)	Injured (x1,000)	Homeless (x1,000)	Killed (x1,000)	Injured (x1,000)	Homeless (x1,000)	Killed (x1,000)	Injured (x1,000)	Homeless (x1,000)
1601	ALGER CENTRE	96.3	0.9	3.1	39	0.2	1.1	11	0.0	0.0	3
1602	SIDI M'HAMED	90.5	0.8	2.8	37	0.1	0.9	9	0.0	0.0	3
1603	EL MADANIA	51.4	0.5	2.1	23	0.1	0.9	8	0.0	0.0	2
1604	HAMMA EL ANNASSER	59.2	0.4	1.8	22	0.1	0.6	7	0.0	0.0	2
1605	BAB EL OUED	87.6	0.5	2.2	28	0.1	0.7	7	0.0	0.0	1
1606	BOLOGHINE	43.3	0.2	1.2	13	0.0	0.0	3	0.0	0.0	1
1607	CASBAH	50.5	0.5	2.1	19	0.1	0.6	5	0.0	0.0	1
1608	OUED KORICHE	53.4	0.4	1.9	20	0.0	0.5	5	0.0	0.0	1
1609	BIR MOURAD RAIS	43.3	0.2	1.1	11	0.0	0.0	3	0.0	0.0	1
1610	EL BIAR	52.6	0.5	2.1	24	0.1	0.6	6	0.0	0.0	2
1611	BOUZAREAH	69.2	0.4	1.7	18	0.0	0.1	3	0.0	0.0	1
1612	BIRKHADEM	55.1	0.3	1.4	16	0.0	0.4	5	0.0	0.0	2
1613	EL HARRACH	48.2	0.4	1.8	22	0.3	1.5	16	0.0	0.4	5
1615	OUED SMAR	21.4	0.1	0.7	8	0.1	0.8	8	0.0	0.0	3
1616	BOUROUBA	77.5	0.5	2.0	30	0.3	1.5	20	0.0	0.5	7
1617	HUSSEIN DEY	49.9	0.5	2.0	23	0.2	1.1	11	0.0	0.2	4
1618	KOUBA	105.3	0.7	2.5	33	0.2	1.3	14	0.0	0.3	4
1619	BACH DJERAH	90.1	0.6	2.4	28	0.3	1.6	16	0.1	0.6	6
1620	DAR EL BEIDA	44.8	0.2	1.3	16	0.3	1.7	21	0.1	0.6	7
1621	BAB EZZOUAR	92.2	0.5	2.1	26	0.5	2.1	27	0.1	0.7	7
1622	BEN AKNOUN	19.4	0.1	0.6	6	0.0	0.0	1	0.0	0.0	0
1623	DELY BRAHIM	30.6	0.1	1.0	10	0.0	0.0	2	0.0	0.0	0
1624	HAMMAMET	19.7	0.1	0.6	6	0.0	0.0	1	0.0	0.0	0
1625	RAIS HAMIDOU	21.5	0.1	0.6	7	0.0	0.0	1	0.0	0.0	0
1626	DJASR KACENTINA	82.7	0.3	1.6	18	0.1	1.0	10	0.0	0.0	3
1627	EL MOURADIA	29.5	0.3	1.5	15	0.0	0.4	5	0.0	0.0	1
1628	HYDRA	35.7	0.2	1.1	10	0.0	0.0	2	0.0	0.0	1
1629	MOHAMMADIA	42.1	0.3	1.5	16	0.2	1.2	12	0.0	0.2	4
1630	BORDJ EL KIFFAN	103.7	0.8	2.9	43	0.8	3.0	46	0.3	1.4	17
1631	EL MAGHARIA	30.5	0.2	1.0	11	0.0	0.5	6	0.0	0.0	2
1632	BENI MESSOUS	17.5	0.1	0.6	6	0.0	0.0	1	0.0	0.0	0
1639	BORDJ EL BAHRI	27.9	0.1	1.0	10	0.2	1.1	12	0.0	0.2	4
1640	EL MARSA	8.8	0.0	0.1	3	0.0	0.2	4	0.0	0.0	1
1644	AIN BENIAN	52.3	0.5	2.1	24	0.0	0.0	3	0.0	0.0	1
Total		1,803.3	12.0	54.7	642	4.6	25.2	311	0.6	5.0	97

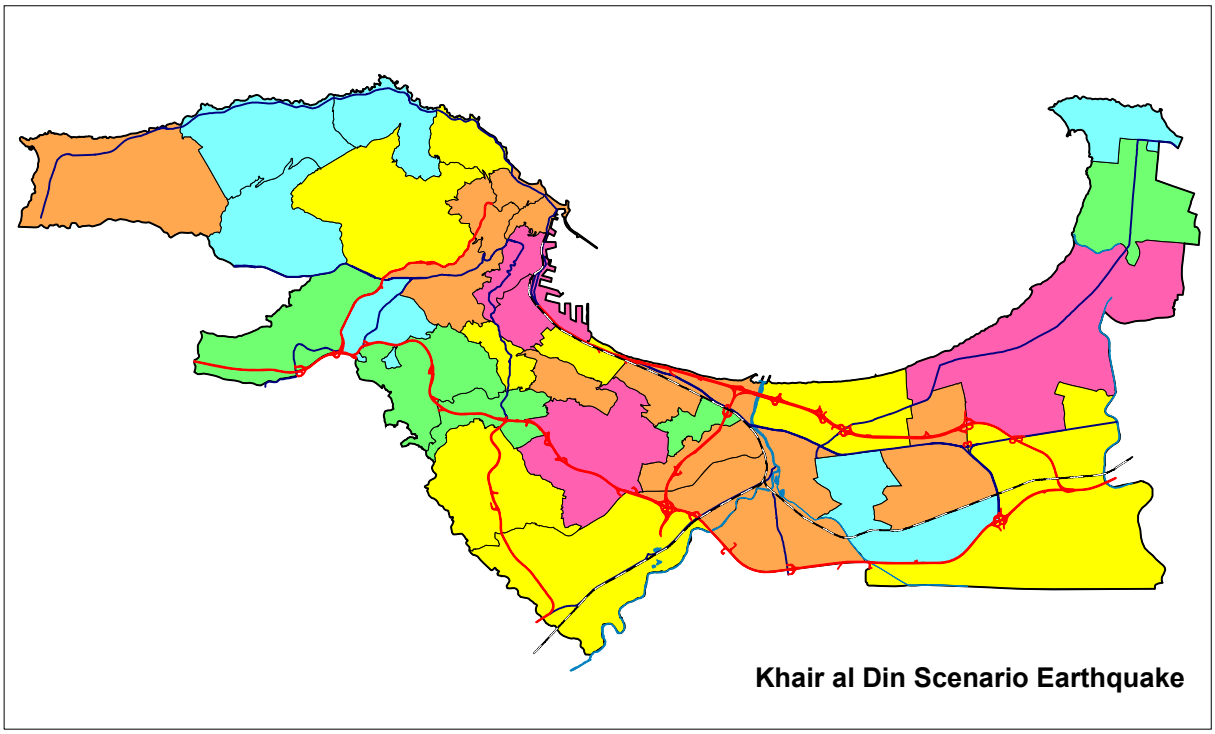

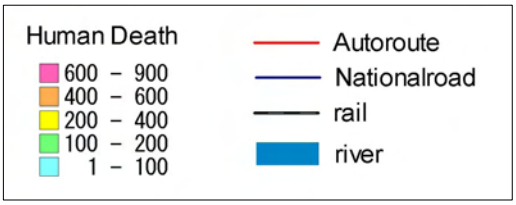

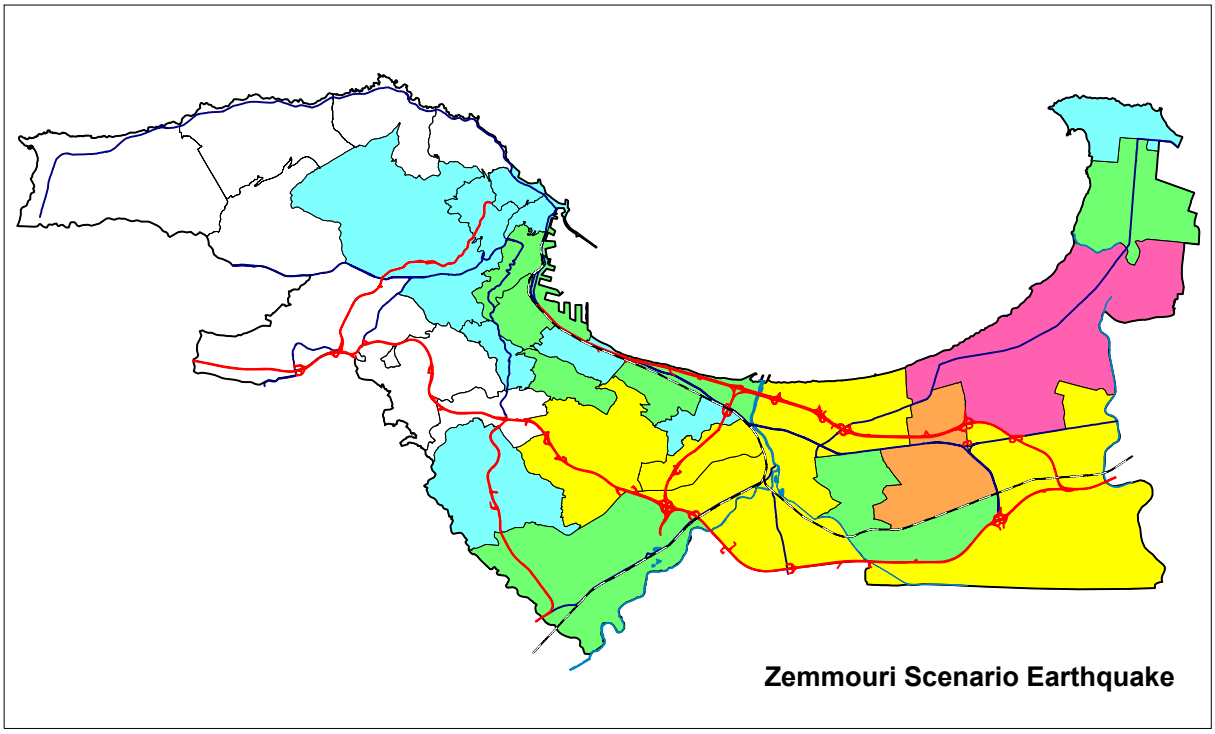

Figure 6-7 Number of Dead